DFT Investigation of the Mechanism of Action of Organoiridium(III) Complexes As Anticancer Agents

ARTICLE *in* INORGANIC CHEMISTRY · OCTOBER 2015

Impact Factor: 4.76 · DOI: 10.1021/acs.inorgchem.5b01832

3 AUTHORS:

Ida Ritacco

Università della Calabria

4 PUBLICATIONS **3** CITATIONS

SEE PROFILE

Nino Russo

Università della Calabria

518 PUBLICATIONS **7,878** CITATIONS

SEE PROFILE

Emilia Sicilia

Università della Calabria

150 PUBLICATIONS **1,894** CITATIONS

SEE PROFILE

Inorganic Chemistry

Article

pubs.acs.org/IC

DFT Investigation of the Mechanism of Action of Organoiridium(III) Complexes As Anticancer Agents

Ida Ritacco, Nino Russo, and Emilia Sicilia*

Dipartimento di Chimica e Tecnologie Chimiche, Università della Calabria, Ponte P. Bucci, Cubo 14cI-87030, Arcavacata di Rende, Italy

Supporting Information

ABSTRACT: The potential use of synthetic metal complexes able to catalyze chemical transformations in living organisms is currently attracting a great deal of attention. Recently, organometallic ruthenium and iridium complexes have revealed an unexpected ability to modulate the redox status of cancer cells. In particular, half-sandwich organoiridium(III) cyclopentadienyl complexes of general formula $[(\eta^5\text{-Cp}^x)\text{Ir(III)-(X^Y)Z}]^{0/+}$, where Cp^x = Cp*, Cp^{xph} (tetramethyl-(phenyl)-cyclopentadienyl) or Cp^{xbiph} (tetramethyl(biphenyl)-cyclopentadienyl), X^Y = bidentate ligand with nitrogen, oxygen, and/or carbon donor atoms, and Z = Cl, H_2O, or pyridine (py) have shown promising antiproliferative activity toward cancer cells, higher potency than cisplatin, and a different mechanism of action due to the increase of the oxidative stress in cells. As such, complexes can belong to the class of DNA interacting compounds and attack on DNA can represent a secondary mechanism of action. We have explored here by means of density functional calculations (M06-L) and with the support of experimental observations for both $[(\eta^5\text{-Cp}^{xbiph})\text{Ir-(phpy) (Cl)}]$, **1-Cl**, and $[(\eta^5\text{-Cp}^{xbiph})\text{Ir-(phpy) (py)}]$, **1-py**, complexes the mechanistic aspects of the hydrolysis reaction, H_2O_2 ROS production by assisted hydride transfer from NADH to molecular oxygen, interaction with purine nucleobases adenine and guanine as well as gluthatione, that is highly abundant in cells, alongside the reaction mechanism for the oxidation of the formed sulfur-coordinated thiolate to the corresponding sulfenato complex. The comparison between kinetic and thermodynamic parameters calculated for all the involved processes shows that, according to the hypothesis based on experimental findings, the interaction with the tripeptide glutathione causes deactivation of **1-Cl**, whereas **1-py**, in both its aquated and nonaquated form, can induce cell apoptosis in a dual manner: DNA damage and H_2O_2 ROS production to increase oxidative stress.

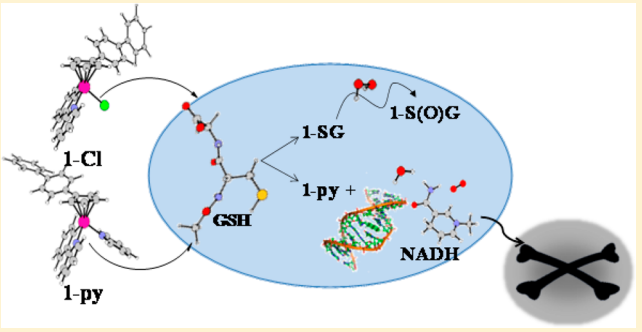

INTRODUCTION

Cisplatin, *cis*-diamminedichloroplatinum(II), was the first Pt-based complex used as an antiproliferative agent and is well-known for its high level and broad spectrum of anticancer activity.[1] Since the serendipitous discovery of the anticancer activity of cisplatin by Rosenberg in the 1960s,[1a] a large number of anticancer Pt(II) drugs have been synthesized and tested for their biological activity,[2] but only a few of them, like carboplatin and oxaliplatin, are used in clinical therapy for applying to various types of cancers.[2a,3] Pt(II)-based anticancer drugs are square-planar d^8 complexes that activated by hydrolysis trigger cancer cell death by binding to nuclear DNA and distorting its structure.[4] However, in spite of their remarkable versatility, side effects of cisplatin and related Pt(II) complexes limit their clinical usefulness and represent a continuing challenge.[5] Both clinical success and drawbacks of Pt antineoplastic compounds have motivated the exploration of non-platinum metal antitumor agents having reduced side effects, lower resistance, and efficacy toward a wider range of cancers and different mechanisms of action (MoA).[6] Over the past decade, increased efforts have been devoted toward targeting redox alterations in cancer[7] because tumors frequently exhibit high oxidative stress with an increased production of reactive oxygen species (ROS). The consequential increased vulnerability of cancer cells to modulations of the ROS homeostasis has therefore been exploited with oxidative stress promoting redox catalysts. Iridium complexes are particularly promising in this respect even if initial efforts have been concentrated on d^8 Ir(I) square−planar complexes in analogy with cisplatin.[8] More recently, encouraging antiproliferative activity toward cancer cells of organometallic complexes of the Ir(III) low-spin d^6 ion have been investigated.[9] Iridium(III) complexes are generally thought to be too inert to possess high reactivity, and even hundreds of years can be required to exchange ligands.[10] However, the introduction of proper ligands can significantly increase the ligands exchange rate and modulate inertness and stability that might also be suitable properties for anticancer drugs.[11] A series of half-sandwich cyclopentadienyl anticancer complexes of general formula $[(\eta^5\text{-Cp}^x)\text{Ir(III)(X^Y)Z}]^{0/+}$,

Received: August 15, 2015

DOI: 10.1021/acs.inorgchem.5b01832
Inorg. Chem. XXXX, XXX, XXX−XXX

where the Cp^x ligand can be a pentamethylcyclopentadienyl (Cp*), phenyltetramethylcyclopentadienyl (Cp^{xph}), or biphenyltetramethylcyclopentadienyl (Cp^{xbiph}) moiety, X^Y is a chelating ligand, and Z is Cl or pyridine (py), has been synthesized and characterized as potential anticancer agents.[12] The general structure of such complexes is shown in Scheme 1.

Scheme 1. General Structure of Ir(III) Cyclopentadienyl Complexes

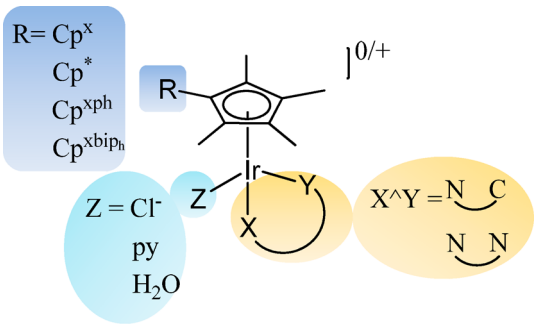

The extended arene in the functionalized Cp* ligand may play a role in interactions with a target. The chelating ligand X^Y affords additional stability to the complex and contributes to tuning the electronic properties of the iridium center. The monodentate ligand Z, such as chloride, can provide a labile site for substitution reactions with target sites.

Very recently, Sadler's group[13] has reported an investigation of the organoiridium(III) complex [(η^5-Cp^{xbiph})Ir-(phpy)(Cl)], containing the C^N-chelated phenylpyridine (phpy) and π-bonded biphenyltetramethylcyclopentadienyl (Cp^{xbiph}) ligands, as a model of a new generation of anticancer drugs, which should cause an increase of the oxidative stress owing to both production of reactive oxygen species (ROS) and diminished ability to scavenge ROS.

On the basis of the results of such investigation, Sadler and co-workers have demonstrated that the organoiridium complex [(η^5-Cp^{xbiph})Ir-(phpy)(Cl)], for which we adopt the same label used in the reference paper, **1-Cl**, undergoes rapid hydrolysis of the chlorido ligand. The pyridine analogue [(η^5-Cp^{xbiph})Ir-(phpy)(py)], synthesized starting from **1-Cl**, instead, hydrolyzes slowly. As a consequence, the authors have hypothesized that replacement of the chlorido ligand with pyridine (py) protects the complex from deactivation. Also, the reaction with the abundant intracellular thiol glutathione (GSH), that is very rapid for the **1-Cl** complex, becomes very slow for the pyridine complex, **1-py**. Evaluation tests of the antiproliferative activity suggest that, even if **1-py** is more potent than **1-Cl**, the MoA of both complexes is different from that of cisplatin and other platinum complexes. Aiming at proving that the anticancer activity of such complexes should be that expected for oxidant drugs, the authors have investigated whether the reaction of **1-py** and **1-Cl** complexes with the coenzyme nicotinamide adenine dinucleotide, NADH, can lead to the production of ROS. The ability of both **1-py** and **1-Cl** to catalytically transfer a hydride from NADH to molecular oxygen forming H_2O_2 has been demonstrated. Such results suggest the primary mechanism of action of this class of iridium complexes to be perturbation of the redox status of cells, whereas attack on DNA and its damage should represent the secondary mechanism. Indeed, the investigation[12c,d] of adduct formation with both 9-ethylguanine (9-EtG) and 9-methyladenine (9-MeA) has shown that the monodentate ligand, such as chloride and py, can provide a labile site for substitution reactions with the potential DNA target site. Finally, very recently, Liu and Sadler have shown that the iridium glutathione adduct, indicated from now on as **1-SG**, formed by substitution of the chlorido or pyridine ligands in **1-Cl** and **1-py**, respectively, by S-bound glutathione can be readily oxidized to the sulfenato complex **1-S(O)G** by H_2O_2 produced via hydride transfer from coenzyme NADH to iridium and then to O_2.[14] The authors suggest that the new adduct can play a role in the anticancer activity of such iridium complexes.

With the aim to elucidate the MoA of **1-Cl** and **1-py** iridium complexes and to rationalize a great deal of experimental data, we have performed density functional theory (DFT) calculations, which can provide valuable information exploitable in optimizing the design of this class of anticancer complexes. For both the **1-Cl** complex and **1-py** analogue, the mechanistic routes of the hydrolysis reaction and H_2O_2 ROS production by hydride transfer from NADH to molecular oxygen have been theoretically explored. Interactions with GSH as well as purine nucleobases adenine (A) and guanine (G) have been also investigated alongside the reaction mechanism for the formed **1-SG** oxidation to **1-S(O)G**. Our study shows that the primary MoA of both **1-Cl** and **1-py** complexes should be the increase of the oxidative stress. According to the hypothesis formulated on the basis of the experimental findings,[13] it seems to be the interaction with the tripeptide glutathione that plays a crucial

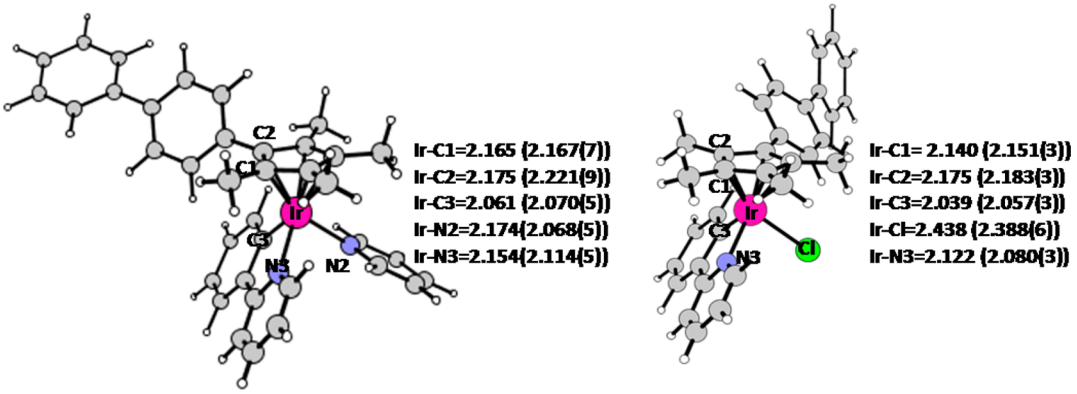

Figure 1. Fully optimized structure of **1-Cl** and cationic portion of **1-py** complexes. Selected bond lengths (in Å) are compared with available experimental values (in parentheses).

DOI: 10.1021/acs.inorgchem.5b01832
Inorg. Chem. XXXX, XXX, XXX−XXX

role in influencing both the fate and the potency of the two complexes, causing deactivation of the **1-Cl** in comparison to the less reactive **1-py**.

RESULTS AND DISCUSSION

M06-L fully optimized structure of the **1-Cl** and **1-py** complexes are shown in Figure 1, where the experimental and theoretical values of the most significant geometrical parameters are compared. Calculated geometrical parameters agree with those extracted from the crystallographic characterization[13,15] of the complexes, indicating a good modeling of the investigated systems. Supporting Information (SI) gives atomic coordinates for the complexes (Table S1).

1. Hydrolysis of Chloride, 1-Cl, and Pyridine, 1-py, Complexes. Given that metal aqua complexes are often more reactive than their equivalent nonaqua complexes and hydrolysis can represent an activation step for transition metal anticancer compunds[12c,16] as for Pt drugs,[17] the ability to undergo hydrolysis of the M−Z bond has been investigated also for half-sandwich cyclopentadienyl anticancer complexes.[13,15] Such studies have shown as the presence of the strongly bound pyridine ligand slows down the hydrolysis reaction by several orders of magnitude compared to that of its chlorido analogue **1-Cl**.

M06-L free energy profiles in solvent for the aquation reaction of the chloride complex **1-Cl** and the corresponding pyridine complex **1-py** are compared in Figure 2. Fully

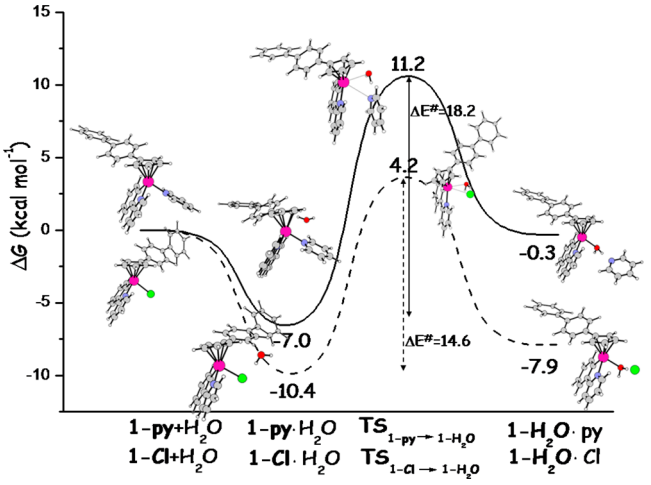

Figure 2. Calculated M06-L free energy profiles in water for the hydrolysis of **1-py** (solid line) and **1-Cl** (dashed line). Energies are in kcal·mol^{-1} and relative to separated reactants.

optimized geometrical structures of all intercepted stationary points are sketched in the same figure. Minima and transition states Cartesian coordinates can be found in the SI. According to the previous theoretical investigations,[18] several water attack modes have been explored and only one of them, the lowest energy one, has been reported. For both complexes, the reaction proceeds by formation of a first adduct in which the water molecule interacts with the chlorine atom of **1-Cl** complex and nitrogen atom of the py ligand in **1-py** complex. Adducts are more stable than separated reactants by 10.4 kcal mol^{-1} in the former case and 7.0 kcal mol^{-1} in the latter. The reaction proceeds by second-order nucleophilic substitution (SN2), that is an exchange of two ligands, the chlorine anion and py, with the water molecule. The transition state structures for the associative displacement of chlorine and py ligands lie 4.2 and 11.2 kcal mol^{-1} above the reactants reference energy, respectively, that is, the barrier that is necessary to overcome is 14.6 kcal mol^{-1} for the displacement of the Cl^- and 18.2 kcal mol^{-1} for the py ligand. The substitution reaction is calculated to be exothermic by 7.9 kcal mol^{-1} for the displacement of chorine anion and almost thermoneutral for the displacement of the py ligand. The hydrolysis reaction of the **1-Cl** complex is calculated to be more favored from both kinetic and thermodynamic points of view according to experimental findings that show how the substitution of the Cl^- ligand with pyridine slows down the rate of the hydrolysis reaction.

Because the methyl groups of the Cp^{xbiph} ligand have been substituted with hydrogen atoms with the purpose to reduce the computational cost, the effects of such substitution have been preliminarily checked. In the SI (Figure S1) is reported a comparison between the energy profiles for chloride and py ligands substitution by water when both biphenyltetramethylcyclopentadienyl (**1***-**Cl** and **1***-**py**) and biphenylcyclopentadienyl (**1-Cl** and **1-py**) ligands are used. Such comparison shows that the presence of methyl groups on the Cp^{xbiph} ligand has little effect on the course of the reaction. The more electrodonating CH_3 groups on the Cp ring increase the lability of the monodentate Z ligand with a consequent lowering of the barriers by about 2 kcal mol^{-1}. However, as can be deduced by both NBO charge analysis (Table S2 in the SI) and molecular electrostatic potential (MEP) calculations (Figure S2) for the four complexes **1***-**Cl**, **1***-**py**, **1-Cl**, and **1-py**, methyl groups on the Cp ligand mainly increase the electron density on both biphenyl substituent and C^N-chelated phenylpyridine ligand. This effect is more evident for the **1-py** complex. As expected, in the region of the Z ligand, the surface of chlorido complexes is much more negative than their pyridine analogues.

2. Interactions with Nucleobases. DNA is usually a potential target for transition metal anticancer drugs, as platinum-based drugs that have chiefly contributed to cancer chemotherapy in the last 30 years.[2] Although it has been proved that the underlying biological effects of **1-Cl**, **1-py**, and analogous half-sandwich Ir(III) complexes do not correlate with that of cisplatin,[12a,b,13] interactions with DNA have been equally well investigated,[12,13] as they should represent one of the factors involved in their mechanism of action.

Because, in analogy with Pt-based anticancer drugs, aqua complexes appear to react more readily with nucleobases,[12c] the interaction of the aqua complex **1-H_2O** with a purine base site of DNA has been studied computationally using adenine and guanine as model reactants. Calculated free energy profiles for the interaction with the **1-H_2O** complex are depicted in Figure 3a for guanine and Figure 3b for adenine. Optimized structures of intermediates and transition states intercepted along the guanine and adenine coordination pathways are shown in the same figures, whereas Cartesian coordinates can be found in Table S1 of the SI. Previous investigations[12d] have shown that Ir metal center reacts with guanine via N7 and forms adenine adducts via both N1 and N7, with the N1 interaction adduct being the major product. In addition, investigated Ir complexes showed a higher affinity for guanine in comparison with adenine. The free energy profiles in Figure 3a show that the interaction with guanine stabilizes the formed adduct by 19.2 kcal mol^{-1}. The transition state for the associative displacement of the water molecule and coordination of guanine through the N7 binding site lies 7.6 kcal mol^{-1} above, whereas the whole process leading to the final N7-coordinated guanine complex

DOI: 10.1021/acs.inorgchem.5b01832
Inorg. Chem. XXXX, XXX, XXX−XXX

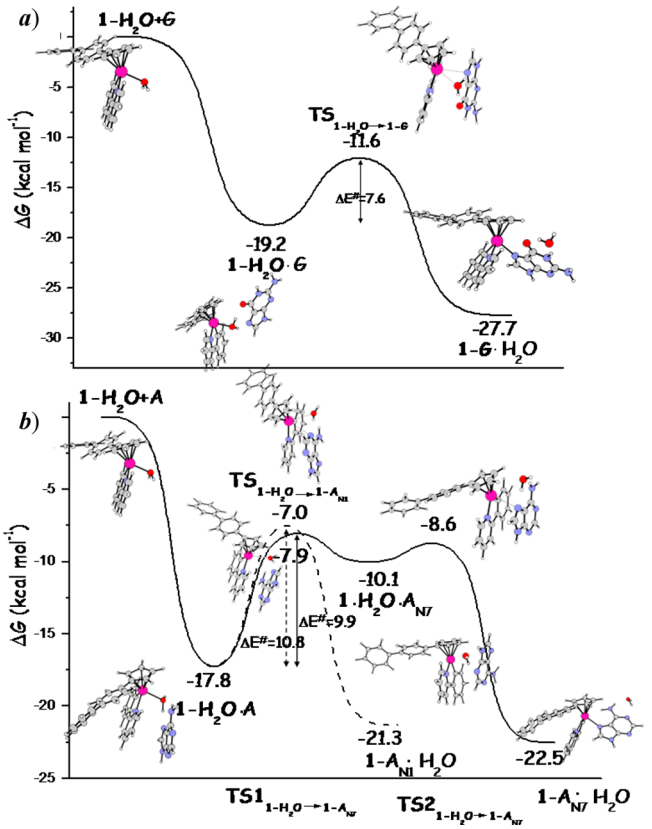

Figure 3. Calculated M06-L free energy profiles in water for the coordination of guanine (a, upper) and adenine (b, lower) to the aqua complex **1-H_2O**. For adenine both N7 (solid line) and N1 (dashed line), coordination sites have been considered. Energies are in kcal·mol^{-1} and relative to separated reactants.

formation is calculated to be exothermic by 27.7 kcal mol^{-1}. Along the analogous pathways for the coordination of adenine, the interaction between the **1-H_2O** complex and adenine leads to the formation of the first intermediate that is stabilized by 17.8 kcal mol^{-1} with respect to reactants' reference energy. Displacement of the water ligand by adenine takes place by following two different mechanisms for binding to N1 and N7 sites: a one-step associative in the former case and a two-step dissociative mechanism in the latter. For the associative displacement of the water molecule and coordination of the N1 site the intercepted transition lies 7.0 kcal mol^{-1} below the entrance channel and then 10.8 kcal mol^{-1} above the first adduct. Product formation is exothermic by 21.3 kcal mol^{-1}. For the dissociative mechanism allowing coordination of the N7 site, the first transition state for the release of H_2O is formed overcoming an energy barrier of 9.9 kcal mol^{-1} and the formed intermediate is calculated more stable by only 2.2 kcal mol^{-1}. The height of the free energy barrier for the next transition state, which allows the N7 site adenine coordination, is only 1.5 kcal mol^{-1}. The process occurs in a stepwise manner even if this region of the surface is very flat. The overall substitution process is exothermic by 22.5 kcal mol^{-1}. The results of our computational analysis do not clearly discriminate between the N1 and N7 modes of coordination neither from a kinetic nor thermodynamic point of view, whereas the preferential binding with guanine in respect to adenine is confirmed.

To check whether the direct interaction of **1-Cl** and **1-py** complexes with nucleobases is less favorable than the interaction of their corresponding aquated complexes, potential energy surfaces (PESs) for the displacement of Cl^- and py ligands and coordination of guanine have been calculated (see Figure 4).

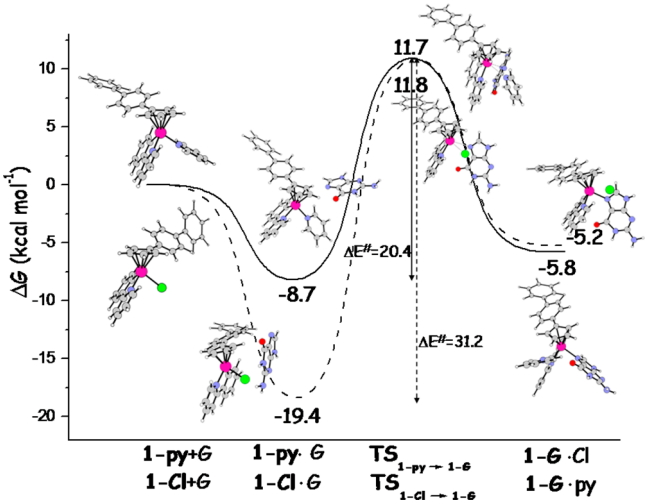

Figure 4. Calculated M06-L free energy profiles in water for guanine coordination to **1-py** (solid line) and **1-Cl** (dashed line). Energies are in kcal·mol^{-1} and relative to separated reactants.

The first formed adduct along the pathway for chloride anion substitution is stabilized by 19.4 kcal mol^{-1} with respect the reference energy of separated reactants, whereas the transition state for the associative guanine substitution lies 11.8 kcal mol^{-1}above. That is, an activation barrier of 31.2 kcal mol^{-1} hampers the displacement process that is calculated to be exothermic by 5.2 kcal mol^{-1}. The relative energies of the first adduct and the transition state for the associative mechanism of displacement with respect to separated reactants along the analogous pathway for the **1-py** complex are −8.7 and 11.7 kcal mol^{-1}, respectively. Therefore, the py ligand substitution takes place overcoming an activation barrier of 20.4 kcal mol^{-1} and leads to the formation of the **1-G** complex that is more stable by 5.8 kcal mol^{-1} than separated reactants. Calculations confirm that, in analogy with other metal anticancer drugs, hydrolysis represents the activation step for DNA binding when the **1-Cl** complex is the cytotoxic agent as the formed **1-H_2O** complex reacts more readily with nucleobases than **1-Cl**. In the case of **1-py**, instead, it is more difficult to select the preferred mechanism. Indeed, the height of the calculated barrier for the activation of **1-py** by hydrolysis, 18.2 kcal mol^{-1}, is only by about 2 kcal mol^{-1} lower than that, of 20.4 kcal mol^{-1}, for the direct guanine coordination by displacement of the py ligand.

3. Reaction with Glutathione Tripeptide. The tripeptide L-glutamyl-L-cysteinyl-glycine (glutathione or GSH) is the most abundant low-molecular-weight thiol containing molecule in human cells and it is believed to form with cisplatin complexes that are a significant cellular sink of the Pt drug, causing its inactivation by forming stable adducts, thus preventing the drug from reaching and binding to DNA.[19] Moreover, reactions of metal complexes with GSH can affect the redox state of cells[20] due to its antioxidant properties, which prevent damage to cellular components caused by reactive oxygen species.[21] Thus, the possible role that could be played

DOI: 10.1021/acs.inorgchem.5b01832
Inorg. Chem. XXXX, XXX, XXX−XXX

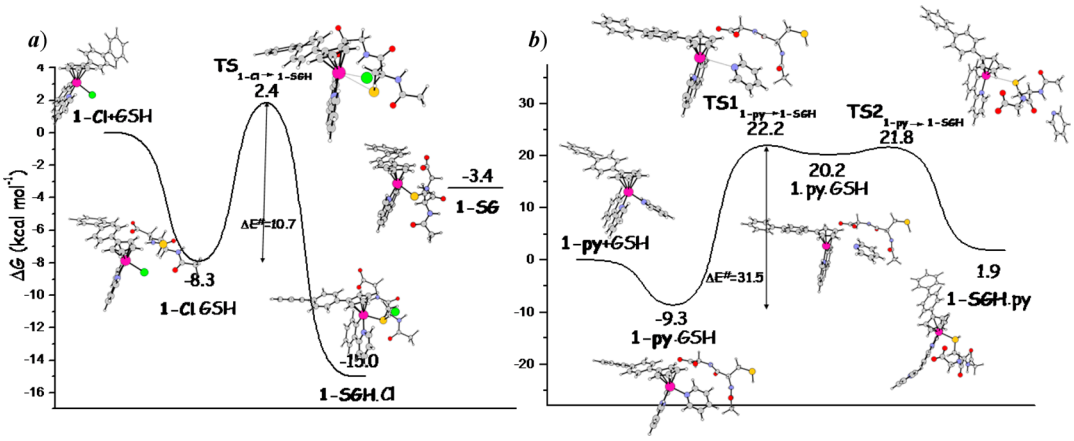

Figure 5. Calculated M06-L free energy profiles in water for the coordination of GSH to the **1-Cl** (a, left) and **1-py** (b, right) complexes. Energies are in kcal·mol^{-1} and relative to separated reactants.

by both GSH in differentiating anticancer activity of **1-Cl** and **1-py** complexes[13] and thiol-mediated redox reactions in the MoA of half-sandwich Ir complexes[15] has been investigated. By substitution of the chlorido and pyridine ligands in the anticancer complexes **1-Cl** and **1-py** with glutathione, the complex $[(\eta^5\text{-Cp}^{xbiph})\text{Ir(phpy) (SG)}]^-$, **1-SG**, is formed. With respect to the reaction of **1-Cl** with GSH, the presence of the py ligand in **1-py** slows down the rate of the substitution reaction by several orders of magnitude.

The outcomes of our exploration of the interaction mechanism of GSH with both **1-Cl** and **1-py** are displayed in Figure 5 for both free energy profiles and stationary point optimized geometries. At physiological pH, the GSH tripeptide assumes zwitterionic form at the glutamyl residue, the cysteine moiety has neutral thiol (SH) side chain and the carboxyl group of the glycine fragment is deprotonated. The computational requirements have been reduced cutting the glutamyl residue. The interaction between **1-Cl** and GSH leads to the formation of an adduct that is more stable than separated reactants by 8.3 kcal mol^{-1}. The favored coordinating mode of GSH to the metal center is through the thiol group that is still protonated. The transition state structure leading to the formation of the HS-bound thiol complex, **1-SGH**, characterized by an imaginary frequency describing the formation of the Ir−S bond and the breaking of the Ir−Cl bond, lies only 2.4 kcal mol^{-1} above the reference energy of dissociated reactants. That means that the free energy barrier for the formation of the substitution product is 10.7 kcal mol^{-1}. The formed product is stabilized by 15.0 kcal mol^{-1} with respect to reactants. Along the analogous pathways for the displacement of the py ligand, the first intermediate is calculated to lie 9.3 kcal mol^{-1} below the entrance channel of the reaction, whereas the substitution of py with GSH proceeds following a dissociative mechanism involving two transition states and a minimum separating them. The height of the barrier to overcome for the first transition state, $\mathbf{TS1}_{\text{1-py→1-SGH}}$, is 31.5 kcal mol^{-1} for the release of the py ligand. The next minimum lies only 2.0 kcal mol^{-1} below the energy of the transition state, leading to it and the barrier of the second transition state, $\mathbf{TS2}_{\text{1-py→1-SGH}}$, for the coordination of glutathione is only 1.6 kcal mol^{-1}. As it clearly appears from Figure 5b, this region of the potential energy profile is very flat and the geometry of the $\mathbf{TS1}_{\text{1-py→1-SGH}}$ transition state is very close to that of the next intermediate. Therefore, as the ligand displacement does not take place in a concerted manner, decoordination of the py ligand represents the slow step that slows down the GSH coordination reaction. The final product lies 1.9 kcal mol^{-1} above the reactants' reference energy. The outcomes of our computations confirm that the energetic cost for the displacement of the py ligand by GSH is remarkably higher than that required to substitute the chloride ligand. Formation of **1-SGH** product complex from **1-Cl** is also favored from a thermodynamic point of view. It is worth emphasizing that, from a comparison of such barriers with the corresponding barriers for the aquation reactions, the glutathione interaction with the **1-Cl** complex involves the lowest energy barrier. Hydrolysis of **1-py**, on the contrary, is more favorable than py ligand displacement by GSH and, mainly, interaction with GSH, much more than aquation, differentiates the behaviors of **1-Cl** and **1-py** complexes.

The final complex **1-SG** is formed by cysteine thiol group SH deprotonation that should be facilitated by coordination to the iridium center also in a nonalkaline medium, as we are going to prove. The equation $\text{GSH}_{(solv)} \rightarrow \text{GS}^-_{(solv)} + \text{H}^+_{(solv)}$ for the isolated glutathione and $\mathbf{1\text{-SGH}}_{(solv)} \rightarrow \mathbf{1\text{-SG}}^-_{(solv)} + \text{H}^+_{(solv)}$ for the HS-bound glutathione complex have been employed together with the experimental value of −269.0 kcal mol^{-1} for the aqueous solvation free energy of the proton, including conversion of the ΔG_{gas} reference state (24.46 L at 298.15 K) from 1 atm to 1 M.[22] The calculated values of the reaction free energy for the equations reported above measuring the deprotonating ability of isolated and Ir-coordinated cysteine thiol − SH group are 14.2 and −3.4 kcal mol^{-1}, respectively, that means about 11 pk_a units.

4. Oxidation of NADH to NAD$^+$ and Generation of ROS. The studies carried out recently by Sadler's group demonstrate that Ir anticancer complexes such those under investigation are able to accept hydride from NADH in aqueous solution and the hydride in turn can be transferred to oxygen to generate H_2O_2.[12a,13] The use of organometallic complexes and intracellular antioxidants allows generating ROS in cancer cells that causing oxidative stress can provide an effective strategy for curing cancer. Experiments have demonstrated that both **1-Cl** and **1-py** are able to accept a hydride from NADH and successively generate the H_2O_2 ROS even if the reaction of **1-py** appears to be slower. The authors have suggested that this difference in behavior maybe due to the difference in hydrolysis rate of the two complexes.

DOI: 10.1021/acs.inorgchem.5b01832
Inorg. Chem. XXXX, XXX, XXX−XXX

Scheme 2. Proposed Mechanisms for Hydride Transfer from MNH to 1-Z Complexes

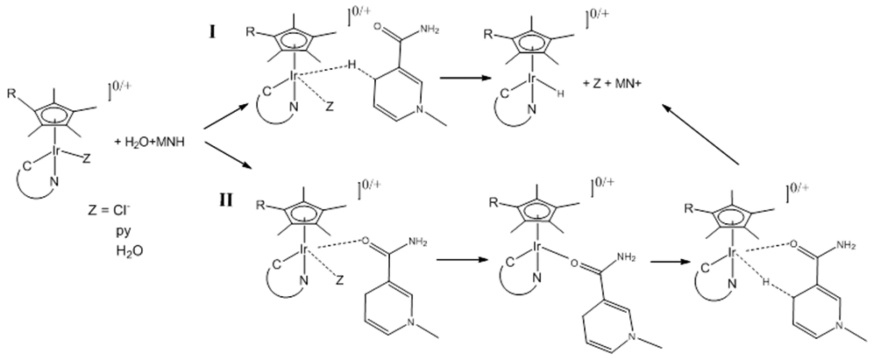

To simulate the hydride transfer reaction from NADH to the **1-Z** complexes (Z = H_2O, Cl, py), two likely mechanisms have been explored (see Scheme 2). Mechanism labeled **I** involves direct transfer of the hydride from NADH to the metal center concomitant to the displacement of the Z ligand. Mechanism labeled **II** occurs in two steps: displacement of the Z ligand and coordination of the carbonyl oxygen of NADH followed by hydride transfer to form the **1-H** complex and the NADH oxidized form NAD^+. Potential energy surfaces calculated at M06-L level for the hydride transfer from NADH to the hydrolyzed complex **1-H_2O** following **I** and **II** mechanisms are shown Figure 6. To reduce the computational cost, the model

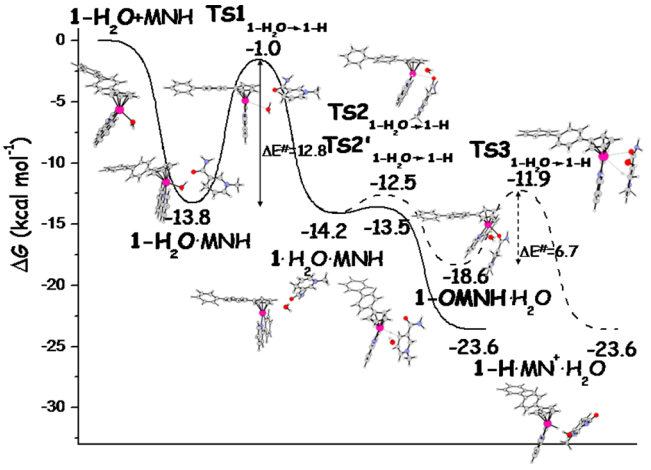

Figure 6. Calculated M06-L free energy profiles in water for the coordination of MNH to the **1-H_2O** along **I** (solid line) and **II** (dashed line) pathways. Energies are in kcal·mol^{-1} and relative to separated reactants.

N-methyl-1,4-dihydronicotinamide, MNH, has been used for mimicking NADH. Analogous calculations carried out for hydride transfer to **1-Cl** and **1-py** are reported and commented below.

Along both **I** and **II** pathways, in the first step, the interaction between **1-H_2O** complex and MNH leads to the formation of the corresponding adduct stabilized by 13.8 kcal mol^{-1} with respect to separated reactants. The next step should be displacement of H_2O and coordination of either the hydride along the path **I** or MNH through the carbonyl oxygen along the path **II**. The substitution occurs following a dissociative mechanism that entails first the elimination of the water molecule overcoming an energy barrier of 12.8 kcal mol^{-1} and formation of a coordinatively unsaturated intermediate that is more stable by only 0.4 kcal mol^{-1} than the previous minimum. Conversion of MNH into its corresponding oxidized form MN^+ through direct hydride transfer to the metal center to form the Ir hydride complex **1-H** requires to occur the overcoming of a very low, only 0.7 kcal mol^{-1}, free energy barrier. The imaginary frequency, calculated to be 282*i* cm^{-1}, corresponds to the movement of the hydrogen atom detaching from carbon and bonding to Ir.

The overall process is calculated to be exothermic by 23.6 kcal mol^{-1}. Along the path **II** for the coordination of the carbonyl oxygen of MNH to the metal center to occur, it is necessary to surmount a very low energy barrier of 1.7 kcal mol^{-1}. The calculated imaginary frequency of 50*i* cm^{-1} describes the movement for the formation of a new Ir−O bond. The formed intermediate is stabilized by 18.6 kcal mol^{-1} with respect to the reference energy and by 4.4 kcal mol^{-1} than the previous minimum. The final step leading to formation of the **1-H** complex takes place with the hydride transfer from the CH_2 moiety of MNH at an energetic cost of 6.7 kcal mol^{-1} for the transition state **$TS3_{1\text{-}H2O\rightarrow 1\text{-}H}$**. From such exploration of the probable mechanisms results that the hydride transfer reaction from NADH to Ir center and formation of NAD^+, very likely, occurs by initial dissociative displacement of the H_2O ligand and direct hydride transfer from the CH_2 group of NADH.

For the sake of completeness, we have carried out analogous calculations for the oxidation of MNH to MN^+ in the presence of **1-Cl** and **1-py** to confirm that, as it is reported in the literature,[8a,23,24] the **1-H_2O** aqua complex is the oxidizing agent that accepts the hydride from MNH. Both mechanisms named **I** and **II** in Scheme 2 have been explored. Calculated free energy profiles for the **II** mechanism are depicted in Figure 7, whereas the mechanism **I** appears to be not viable because water competes for coordination and substitution of Cl^- and py ligands with a water molecule occurs in state of the hydride transfer. Along path **II** the first step is adduct formation that occurs with an energy gain of 28.2 kcal mol^{-1} for **1-Cl** and 17.3 kcal mol^{-1} for **1-py**. Next, the second-order nucleophilic substitution of chloride and pyridine ligands and formation of a new Ir−O bond with the carbonyl oxygen of MNH takes place. The activation energies are calculated to be 14.8 and 15.1 kcal mol^{-1} for the **1-Cl** and **1-py** complexes, respectively. The formed intermediates lye 22.4 and 10.7 kcal mol^{-1} below the entrance channel for Cl^- and py substitution, respectively. The subsequent decoordination of MNH and hydride transfer from the CH_2 group to the metal center to form MN^+ requires 5.9 and 8.2 kcal mol^{-1} along the pathways starting from the **1-Cl** and **1-py** complexes, respectively. The product of the process, the iridium hydride complex **1-H**, lies 25.6 and 23.4 kcal mol^{-1}

DOI: 10.1021/acs.inorgchem.5b01832
Inorg. Chem. XXXX, XXX, XXX−XXX

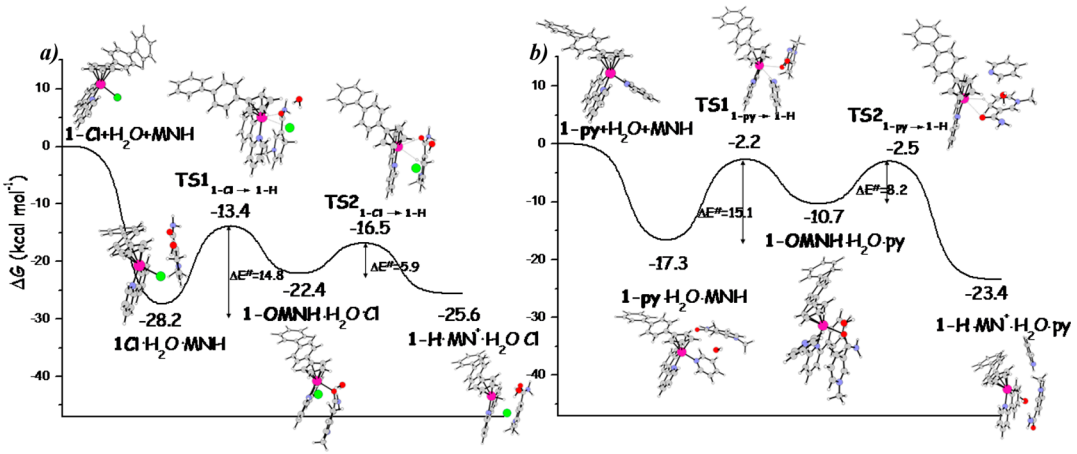

Figure 7. . Calculated M06-L free energy profiles in water for the coordination of MNH to the **1-Cl** (a left) and **1-py** (b right) along the pathway named **II**. Energies are in kcal·mol^{-1} and relative to separated reactants.

below the reference energy of separated **1-Cl** and **1-py** reactants, respectively.

To summarize, the **1-H$_2$O** aqua complex interacts with NADH, modeled by MNH, for the hydride transfer and formation of the corresponding hydride complex more favorably than **1-Cl** and **1-py** complexes. The difference in the activation energies for aquation is therefore responsible for the observed difference in the rates of NADH oxidation reaction for the two complexes. If the direct interaction of **1-Cl** and **1-py** complexes with NADH is taken into consideration, the stepwise oxidation described in Figure 7 is calculated to be, in any case, more favorable for **1-Cl**.

Once the **1-H** complex is formed in the presence of molecular oxygen, the ROS H_2O_2 can be produced. Both singlet and triplet M06-L PESs for the oxygenation process of **1-H** are drawn in Figure 8. For the triplet multiplicity, only

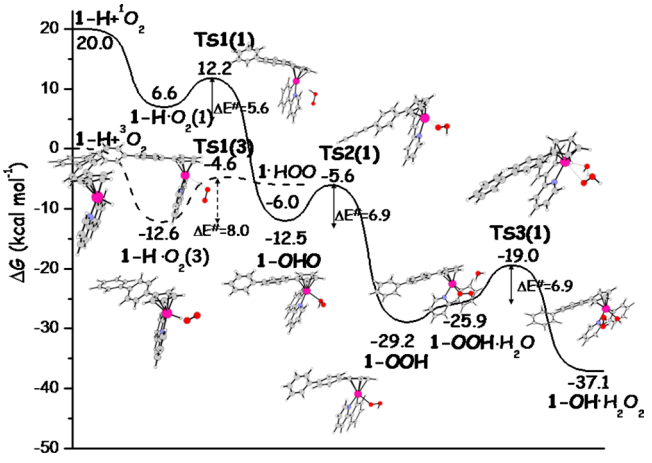

Figure 8. Singlet and triplet calculated M06-L PESs in water solvent for the oxygenation process of **1-H** to produce the H_2O_2 ROS. Energies are in kcal·mol^{-1} and relative to **1-H** + $^3O_2$ ground state reactants.

stationary points involved in the surface crossing are displayed. Cartesian coordinates can be found in the SI (see Table S1). Relative free energies in solution have been calculated with respect to the ground-state reactants asymptote **1-H** + $^3O_2$.

The addition of triplet molecular oxygen yields the adduct **1-H**·O_2(3), whose formation is exothermic by 12.6 kcal mol^{-1}. The optimized structure of the corresponding complex in a singlet state **1-H**·O_2(1) lies at 6.6 kcal mol^{-1} above the entrance channel of separated reactants. The next step of the process involves the abstraction of the hydrogen atom from the iridium center by O_2. Along the triplet pathway, the activation barrier of 8.0 kcal mol^{-1} corresponds to the formation of the **TS1**(3) transition state. The imaginary frequency, calculated to be 1207*i* cm^{-1}, corresponds to the movement of the hydrogen atom detaching from Ir and bonding to the next oxygen. As a result, an intermediate is formed, **1**·(HOO), that lies 1.4 kcal mol^{-1} below the **TS1**(**3**), in which the peroxyl HOO radical is coordinating with the metal center of the complex through a weak interaction between Ir and hydrogen atoms. On the other hand, along the singlet pathway, a transition state, **TS1**(**1**), is intercepted and characterized where the distance between the hydrogen atom and the closest oxygen is 1.361 Å. This transition state lies 12.2 kcal mol^{-1} above the reactants' reference energy and is characterized by an imaginary frequency of 773*i* cm^{-1}. The reaction proceeds with the formation of the intermediate **1**-(**OHO**), whose formation is exothermic by 12.5 kcal mol^{-1}. The most important feature of this intermediate, in analogy with our previous theoretical investigations,[25] is that the hydrogen atom is bonded to the proximal oxygen, whereas the distal oxygen atom is rotated upward. Because the singlet structure of the **1**-(**OHO**) complex is more stable than the **1**-(**OOH**) triplet intermediate, in this region of the PES, a spin inversion has to occur after the passage of the **TS1**(**3**) transition state. However, such a kind of spin crossing occurring after formation of the transition state does not play a critical role in influencing the rate of the reaction.[26]

After the crossing, the reaction proceeds along the singlet path with the formation of the final Ir−hydroperoxo complex and the overall process is calculated to be exothermic by 29.2 kcal mol^{-1}. The reaction evolves through the breaking of the bond between the proximal oxygen and the Ir center that makes a new bond with the distal oxygen. The corresponding transition state **TS2**(**1**), lying 5.6 kcal/mol below the reactants dissociation limit, has been intercepted and confirmed by IRC analysis.

The last step of the process leads to the release of H_2O_2 from the hydroperoxide complex. Generation and release of hydrogen peroxide is simulated by considering the interaction with an additional explicit water molecule that interacts with the complex causing a destabilization of 3.3 kcal mol^{-1}. The

DOI: 10.1021/acs.inorgchem.5b01832
Inorg. Chem. XXXX, XXX, XXX−XXX

water oxygen atom coordinates to the metal center and simultaneously transfers one of the H atoms to the OOH group. The height of the barrier for this rearrangement is 6.9 kcal mol^{-1} with respect to the energy of the H_2O and hydroperoxide adduct leading to it. The imaginary frequency that confirms the nature of this stationary point is 199*i* cm^{-1} and corresponds to the simultaneous shift of one of the water hydrogen atoms to oxygen to yield a H_2O_2 molecule and form a new bond between the Ir center and the OH^- moiety. The overall process that leads to the production of the H_2O_2 ROS together with formation of a hydroxide complex is exothermic by 37.1 kcal mol^{-1}. As suggested by the authors, in the presence of acidic species a water molecule should be released and the initial Ir complex regenerated.

5. Oxidation of the Ir-SG Complex to the Sulfenato Ir−S(O)G Complex. Very recently, Sadler and co-workers have reported that the formation of the complex **Ir-SG** by substitution of the chlorido and pyridine ligands in the anticancer complexes **Ir-Cl** and **Ir-py** with glutathione can explain the observed differences in potency.[14] The addition of NADH to a solution containing 95% **Ir-SG** and 5% **Ir-py** causes the oxidation of NADH to NAD^+ and subsequent oxidation of the **1-SG** complex to the corresponding sulfenato $[(\eta^5\text{-}Cp^{xbiph})Ir\text{-}(phpy)S(O)G]^-$, **1-S(O)G**, complex.

Here are illustrated the outcomes of the calculation of the PES, reported in Figure 9, describing the oxidation of the **1-SG** complex by the produced H_2O_2 ROS.

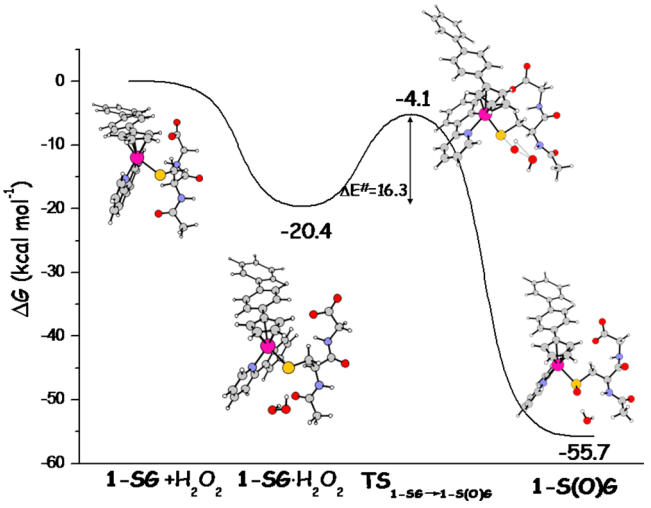

Figure 9. M06-L PES for the oxidation of the **1-SG** complex by the H_2O_2 ROS. Energies are in kcal·mol^{-1} and relative to separated reactants.

The interaction of the sulfur-coordinated thiolate **1-SG** complex with H_2O_2 leads to a stabilization of the corresponding adduct, **1-SG·H_2O_2**, by 20.4 kcal mol^{-1} with respect to the entrance channel. The next step is the conversion of the thiolate adduct to the sulfenato complex **1-S(O)G**, occurring by transfer of one of the oxygen atoms of H_2O_2 to the sulfur atom concomitant to formation of H_2O. The height of the barrier for such rearrangement is 16.3 kcal mol^{-1}, whereas the sulfenato product is formed with an energy gain of 55.7 kcal mol^{-1}. The outcomes of our computations corroborate the hypothesis that the gluthatione complex formed by substitution of the chloride or pyridine ligands in half-sandwich **1-Cl** and **1-py** complexes, respectively by S-bound gluthatione might be not a dead-end product. Owing to driving force of the process, that is, the large calculated exothermicity, the **1-SG** complex can be quite rapidly oxidized and the formed hydrogen peroxide, which should be responsible of the increased ROS oxidative stress in cancer cells as a new strategy for curing cancer, consumed.

6. MoA of Half-Sandwich Cyclopentadienyl 1-Cl and 1-py Anticancer Complexes. All the outcomes of our computational analysis of the water reactivity of the two **1-Cl** and **1-py** complexes illustrated in the previous sections can serve to draw some general conclusions about their MoA as anticancer drugs and to rationalize the observed differences in behavior, mainly the higher potency of **1-py** with respect **1-Cl**.

First, the hydrolysis, that is very often the necessary activation step for metal-based anticancer drugs preluding to the interaction with biological targets, has been examined. Both **1-Cl** and **1-py** complexes undergo hydrolysis even if the substitution of Cl^- in **1-Cl** by water proceeds more rapidly and is more exothermic. The interaction of the formed aqua complex **1-H_2O** with a purine base site of DNA has been studied computationally using adenine and guanine as model reactants. Calculations confirm that the aqua complex readily binds to both purines. As direct interaction of **1-Cl** with guanine is hampered by a very high energy barrier, hydrolysis represents the activation step for DNA binding when the **1-Cl** complex is the cytotoxic agent. The barriers, instead, that are necessary to overcome for the displacement of py ligand in **1-py** by water, is by only 2 kcal mol^{-1} lower than that for guanine.

The process that really differentiates the behaviors of the two complexes and can influence their fate and potency is the interaction with gluthatione. Indeed, the energetic cost for the displacement of the py ligand by gluthatione is remarkably higher (31.5 kcal mol^{-1}) than that required to substitute the chloride ligand (10.7 kcal mol^{-1}) and formation of the corresponding **1-SG** product complex from **1-Cl** is also favored from a thermodynamic point of view. Deactivation of **1-Cl** by gluthatione appears, therefore, to be very likely.

The **1-H_2O** aqua complex as well as **1-Cl** and **1-py** are able to accept a hydride from NADH, causing its conversion into its oxidized form NAD^+. The activation by water and subsequent hydride transfer from the aqua complex is the preferred reaction pathway. The formed hydride complex reacts with triplet molecular oxygen to form the corresponding hyroperoxide complex and after that to release hydrogen peroxide by surmounting low energy barriers. The process involves a surface crossing that does not represent a bottleneck for the reaction.

At last, the oxidation reaction of the formed **1-SG** complex by H_2O_2 has been calculated to occur easily enough consuming the produced ROS hydrogen peroxide that should be the species responsible of the increased oxidative stress in cells.

In summary, it is very likely deactivation of **1-Cl** to occur by interaction with gluthatione, whereas the **1-py** complex does not undergo analogous deactivation and can, both in its aquated and nonaquated form, induce apoptosis in dual manner: by both DNA damage and H_2O_2 ROS production to increase oxidative stress.

CONCLUSIONS

On the basis of the experimental observations and formulated hypotheses on the mechanism of action, we have theoretically investigated with the aid of the density functional theory calculations the aqueous chemistry of the two half-sandwich organoiridium(III) cyclopentadienyl complexes **1-Cl** and **1-py**. The mechanism of the hydrolysis reaction, H_2O_2 ROS

DOI: 10.1021/acs.inorgchem.5b01832
Inorg. Chem. XXXX, XXX, XXX−XXX

production by hydride transfer from NADH to molecular oxygen, interaction with gluthatione and purine nucleobases adenine and guanine alongside the reaction mechanism for the oxidation of the formed sulfur-coordinated thiolate to the corresponding sulfenato complex, have been studied in detail. From the outcomes of our computational analysis, we can assume that the process clearly differentiating the behaviors of the two complexes is the interaction with gluthatione tripeptide. Coordination of gluthatione that occurs very rapidly for the **1-Cl** complex causes its deactivation, whereas a very high energy barrier hampers the process in the case of **1-py**. Both complexes can undergo hydrolysis that leads to the formation of the corresponding aqua complex. For the 1-Cl complex, in analogy with other metal-based anticancer agents, aquation represents the necessary activation step allowing coordination of purine guanine and adenine bases, whereas for **1-py**, the barrier for the aquation is lower than that for guanine coordination by only 2 kcal mol^{-1}. Interaction with NADH to form the corresponding hydride complex occurs preferentially with the aqua complex even if direct interaction with **1-Cl** and **1-py** cannot be excluded. Reaction of the formed hydride with molecular oxygen leads to the production of H_2O_2 ROS, that should be the real cytotoxic agent but that could be consumed to oxidize the formed gluthatione adduct into the corresponding sulfenato complex. Deactivation of **1-Cl** appears to be very likely. The **1-py** action, instead, is not disturbed by gluthatione interaction and can induce cell apoptosis by both DNA damage and H_2O_2 ROS production.

COMPUTATIONAL DETAILS

All molecular geometries were optimized using Truhlar's meta-GGA functional M06-L[27] that was designed to be as good as possible for the study of organometallic systems.[27] Frequency calculations at the same level of theory were also performed to identify all stationary points as minima (zero imaginary frequencies) or transition states (one imaginary frequency). The involved transition states were checked by IRC (intrinsic reaction coordinate) analysis.[28−30] For Ir, the relativistic compact Stuttgart/Dresden effective core potential[31] was used in conjunction with the split valence basis set, while the standard triple-ζ quality basis sets 6-311+G** basis sets of Pople and coworkers were used for the atoms directly participating in the process. For peripheral C and H atoms of both xbiph and phpy, the smaller 6-31G basis sets were used. All the calculations have been carried out employing the Gaussian09 software package.[32]

To reduce the computational cost, the methyl groups of the Cp^{xbiph} ligand were substituted with hydrogen atoms. Therefore, because preliminary calculations have clearly shown that the replacement of methyl groups with hydrogen atoms does not introduce any significant change in energetics, simplified models were adopted for all the studied complexes. Along the pathway for the hydride transfer from NADH to triplet molecular oxygen assisted by iridium complexes, both triplet and singlet multiplicities were examined for all the involved species. $\langle S^2 \rangle$ values were checked to assess whether spin contamination can influence the quality of the results. The method proposed by Ovchinnikov and Labanowski[33] was used for correcting the mixed spin energies and removing the foreign spin components for singlet structures that appeared to be contaminated. For molecular oxygen, for example, the adoption of the mentioned correction scheme, allowed correction of the contaminated singlet wave function and calculate a triplet-singlet energy gap of O_2 of 20.0 kcal mol^{-1}, which is in good agreement with the experimental value.[34]

The impact of solvation effects on the energy profiles was estimated by using the Tomasi's implicit polarizable continuum model (PCM)[35] as implemented in Gaussian09. The UFF set of radii was used to build up the cavity. The solvation Gibbs free energies were calculated in implicit water (ε = 78.4) at the same level by performing single-point calculations on all stationary points structures obtained from vacuum calculations. Enthalpies and Gibbs free energies were obtained at 298 K at 1 atm from total energies, including zero-point, thermal, and solvent corrections, using standard statistical procedures.[36] However, such an approach does not reflect the real entropic change that occurs when the solute goes from the gas to the condensed phase, and the effects are more relevant when association and dissociation are involved. Therefore, following the procedure proposed by Wertz[37] and successfully adopted formerly[38] to properly handle the change of translational and rotational entropy occurring when a solute is transferred from the gas phase into the solution phase, Gibbs free energies in solution for each species, have been calculated as

$$G_{298K} = E_{elec} + G_{solv} + ZPE + H_{vib} + 6kT - T(S_{vib}) - T[0.54 \times (S_{rot} + S_{trans} - 14.3) + 8.0] \quad (1)$$

where T = 298 K and the term $6kT$ accounts for the potential and kinetic energies of the translational and rotational modes. More details can be found in the Supporting Information.

NBO charge analysis[39] and electrostatic potential calculation were carried out on the structures of some intercepted stationary points.

ASSOCIATED CONTENT

Supporting Information

The Supporting Information is available free of charge on the ACS Publications website at DOI: 10.1021/acs.inorgchem.5b01832.

Cartesian coordinates (Å) and absolute energies (Hartrees) of all optimized structures; additional energy profiles; NBO charge analysis; maps of the molecular electrostatic potential (PDF)

AUTHOR INFORMATION

Corresponding Author

*E-mail: siciliae@unical.it.

Notes

The authors declare no competing financial interest.

ACKNOWLEDGMENTS

This research was supported by Università della Calabria.

REFERENCES

(1) (a) Rosenberg, B.; Van Camp, L.; Krigas, T. *Nature* **1965**, *205*, 698−699. (b) Rosenberg, B. In *Cisplatin: Chemistry and Biochemistry of a Leading Anticancer Drug*; Lippert, B., Ed.; Verlag Helvetica Chimica Acta: Zurich, 1999; Part 4, p 3. (c) Cohen, S. M.; Lippard, S. J. *Prog. Nucleic Acid Res. Mol. Biol.* **2001**, *67*, 93−130. (d) Alderden, R. A.; Hall, M. D.; Hambley, T. W. *J. Chem. Educ.* **2006**, *83*, 728−734.

(2) (a) Weiss, R. B.; Christian, M. C. *Drugs* **1993**, *46*, 360−377. (b) Hambley, T. W. *Coord. Chem. Rev.* **1997**, *166*, 181−223. (c) Wong, E.; Giandomenico, C. M. *Chem. Rev.* **1999**, *99*, 2451−2466. (d) Boulikas, T.; Pantos, A.; Bellis, E.; Christofis, P. *Cancer Ther.* **2007**, *S*, 537−583. (e) Reedijk, J. *Pure Appl. Chem.* **2011**, *83*, 1709−1719. (e1) Kelland, L. *Nat. Rev. Cancer* **2007**, *7*, 573−584. (f) Monneret, C. *Ann. Pharm. Fr.* **2011**, *69*, 286−295.

(3) Siddik, Z. *Oncogene* **2003**, *22*, 7265−7279.

(4) (a) Sherman, S. E.; Lippard, S. J. *Chem. Rev.* **1987**, *87*, 1153−1181. (b) Reedijk, J. *Proc. Natl. Acad. Sci. U. S. A.* **2003**, *100*, 3611−3616. (c) Bruijnincx, P. C. A.; Sadler, P. J. *Curr. Opin. Chem. Biol.* **2008**, *12*, 197−206.

(5) (a) Garbutcheon-Singh, K. B.; Grant, M. P.; Harper, B. W.; Krause-Heuer, A. M.; Manohar, M.; Orkey, N.; Aldrich-Wright, J. R. *Curr. Top. Med. Chem.* **2011**, *11*, 521−542. (b) Hannon, M. J. *Pure Appl. Chem.* **2007**, *79*, 2243−2261. (c) Fu, Y.; Habtemariam, A.; Pizarro, A. M.; Van Rijt, S. H.; Healey, D. J.; Cooper, P. A.; Shnyder, S. D.; Clarkson, G. J.; Sadler, P. J. *J. Med. Chem.* **2010**, *53*, 8192−8196.

DOI: 10.1021/acs.inorgchem.5b01832
Inorg. Chem. XXXX, XXX, XXX−XXX

(d) Fu, Y.; Habtemariam, A.; Basri, A. M. B. H.; Braddick, D.; Clarkson, G. J.; Sadler, P. J. *Dalton Trans.* **2011**, *40*, 10553−10562. (e) Park, G. Y.; Wilson, J. J.; Song, Y.; Lippard, S. J. *Proc. Natl. Acad. Sci. U. S. A.* **2012**, *109*, 11987−11992. (f) Pracharova, J.; Zerzankova, L.; Stepankova, J.; Novakova, O.; Farrer, N. J.; Sadler, P. J.; Brabec, V.; Kasparkova. *Chem. Res. Toxicol.* **2012**, *25*, 1099−1111. (g) Castonguay, A.; Doucet, C.; Juhas, M.; Maysinger, D. *J. Med. Chem.* **2012**, *55*, 8799−8806. (h) Hartinger, C. G.; Phillips, A. D.; Nazarov, A. A. *Curr. Top. Med. Chem.* **2011**, *11*, 2688−2702. (i) Liu, Z.; Habtemariam, A.; Pizarro, A. M.; Fletcher, S. A.; Kisova, A.; Vrana, O.; Salassa, L.; Bruijnincx, P. C. A.; Clarkson, G. J.; Brabec, V.; Sadler, P. J. *J. Med. Chem.* **2011**, *54*, 3011−3026.

(6) (a) Giraldi, T.; Sava, G.; Mestroni, G.; Zassinovich, G.; Stolfa, D. *Chem.-Biol. Interact.* **1978**, *22*, 231−238. Sava, G.; Zorzet, S.; Perissin, L.; Mestroni, G.; Zassinovich, G.; Bontempi, A. *Inorg. Chim. Acta* **1987**, *137*, 69−71.

(7) Trachootham, D.; Alexandre, J.; Huang, P. *Nat. Rev. Drug Discovery* **2009**, *8*, 579−591.

(8) (a) Liu, Z.; Sadler, P. J. *Acc. Chem. Res.* **2014**, *47*, 1174−1185. (b) Wirth, S.; Rohbogner, C.; Cieslak, M.; Kazmierczak-Baranska, J.; Donevski, S.; Nawrot, B.; Lorenz, I.-P. *JBIC, J. Biol. Inorg. Chem.* **2010**, *15*, 429−440. (c) Casini, A.; Edafe, F.; Erlandsson, M.; Gonsalvi, L.; Ciancetta, A.; Re, N.; Ienco, A.; Messori, L.; Peruzzini, M.; Dyson, P. J. *Dalton Trans.* **2010**, *39*, 5556−5563. (d) Gras, M.; Therrien, B.; Süss-Fink, G.; Casini, A.; Edafe, F.; Dyson, P. J. *J. Organomet. Chem.* **2010**, *695*, 1119−1125. (e) Ruiz, J.; Rodriguez, V.; Cutillas, N.; Samper, K. G.; Capdevila, M.; Palacios, O.; Espinosa, A. *Dalton Trans.* **2012**, *41*, 12847−12856. (f) Lo, K. K.-W.; Zhang, K. Y. *RSC Adv.* **2012**, *2*, 12069−12083. (g) Gasser, G.; Ott, I.; Metzler-Nolte, N. *J. Med. Chem.* **2011**, *54*, 3−25.

(9) (a) Wilbuer, A.; Vlecken, D. H.; Schmitz, D. J.; Kräling, K.; Harms, K.; Bagowski, C. P.; Meggers, E. *Angew. Chem., Int. Ed.* **2010**, *49*, 3839−3842. (b) Messori, L.; Marcon, G.; Orioli, P.; Fontani, M.; Zanello, P.; Bergamo, A.; Sava, G.; Mura, P. *J. Inorg. Biochem.* **2003**, *95*, 37−46. (c) Marcon, G.; Casini, A.; Mura, P.; Messori, L.; Bergamo, A.; Orioli, P. *Metal-Based Drugs* **2000**, *7*, 195−200.

(10) Cusanelli, A.; Frey, U.; Richens, D. T.; Merbach, A. E. *J. Am. Chem. Soc.* **1996**, *118*, 5265−5271.

(11) Poth, T.; Paulus, H.; Elias, H.; Dücker-Benfer, C.; van Eldik, R. *Eur. J. Inorg. Chem.* **2001**, *2001*, 1361−1369.

(12) (a) Liu, Z.; Sadler, P. J. *Acc. Chem. Res.* **2014**, *47*, 1174−1185. (b) Hearn, J.; Romero-Canelón, I.; Qamar, B.; Liu, Z.; Hands-Portman, I.; Sadler, P. J. *ACS Chem. Biol.* **2013**, *8*, 1335−1343. (c) Liu, Z.; Habtemariam, A.; Pizarro, A. M.; Fletcher, S. A.; Kisova, A.; Vrana, O.; Salassa, L.; Bruijnincx, P. C. A.; Clarkson, G. J.; Brabec, V.; Sadler, P. J. *J. Med. Chem.* **2011**, *54*, 3011−3026. (d) Liu, Z.; Salassa, L.; Habtemariam, A.; Pizarro, A. M.; Clarkson, G. J.; Sadler, P. J. *Inorg. Chem.* **2011**, *50*, 5777−5783. (e) Liu, Z.; Romero-Canelón, I.; Habtemariam, A.; Clarkson, G. J.; Sadler, P. J. *Organometallics* **2014**, *33*, 5324−5333. (f) Ali Nazif, M.; Bangert, J.-A.; Ott, I.; Gust, R.; Stoll, R.; Sheldrick, W. S. *J. Inorg. Biochem.* **2009**, *103*, 1405−1414.

(13) Liu, Z.; Romero-Canelón, I.; Qamar, B.; Hearn, J. M.; Habtemariam, A.; Barry, N. P. E.; Pizarro, A. M.; Clarkson, G. J.; Sadler, P. J. *Angew. Chem., Int. Ed.* **2014**, *53*, 3941−3946.

(14) Liu, Z.; Sadler, P. J. *Inorg. Chem. Front.* **2014**, *1*, 668−672.

(15) Liu, Z.; Habtemariam, A.; Pizarro, A. M.; Clarkson, G. J.; Sadler, P. J. *Organometallics* **2011**, *30*, 4702−4710.

(16) (a) Martin, R. B. In *Cisplatin: Chemistry and Biochemistry of a Leading Anticancer Drug*; Lippert, B., Ed.; Verlag Helvetica Chimica Acta: Zurich, 1999; pp 181−205. (b) Hohmann, H.; Hellquist, B.; van Eldik, R. *Inorg. Chem.* **1992**, *31*, 345−351.

(17) Pizarro, A. M.; Habtemariam, A.; Sadler, P. J. In *Medicinal Organometallic Chemistry*, 1st ed.; Topics in Organometallic Chemistry; Jaouen, G., Metzler-Nolte, N., Eds.; Springer-Verlag: Heidelberg, Germany, 2010; Vol. *32*, pp 21−56.

(18) Wang, H. L.; De Yonker, N. J.; Gao, H.; Tan, C. P.; Zhang, X. T.; Ji, L. N.; Zhao, C. Y.; Mao, Z. W. *RSC Adv.* **2012**, *2*, 436−446.

(19) (a) Dolphin, D.; Avramović, O.; Poulson, R. *Glutathione: Chemical, Biochemical, And Medical Aspects*; Wiley, New York, 1989;. (b) Hwang, C.; Sinskey, A. J.; Lodish, H. F. *Science* **1992**, *257*, 1496−1502. (c) Corazza, A.; Harvey, I.; Sadler, P. J. *Eur. J. Biochem.* **1996**, *236*, 697−705. (d) Bibhesh, K. S. *Asian J. Chem.* **2005**, *17*, 1−32. (e) Zhang, K.; Mack, P.; Wong, K. P. *Int. J. Oncol.* **1998**, *12*, 871−882.

(20) (a) Valko, M.; Morris, H.; Cronin, M. T. D. *Curr. Med. Chem.* **2005**, *12*, 1161−1208. (b) Romero-Canelón, I.; Sadler, P. J. *Inorg. Chem.* **2013**, *52*, 12276−12291.

(21) Sies, H. *Free Radical Biol. Med.* **1999**, *27*, 916−921.

(22) Liptak, M. D.; Shields, G. C. *J. Am. Chem. Soc.* **2001**, *123*, 7314−7319.

(23) Betanzos-Lara, S.; Liu, Z.; Habtemariam, A.; Pizarro, A. M.; Qamar, B.; Sadler, P. J. *Angew. Chem., Int. Ed.* **2012**, *51*, 3897−3900.

(24) Liu, Z.; Deeth, R. J.; Butler, J. S.; Habtemariam, A.; Newton, M. E.; Sadler, P. J. *Angew. Chem., Int. Ed.* **2013**, *52*, 4194−4197.

(25) Chowdhury, S.; Himo, F.; Russo, N.; Sicilia, E. *J. Am. Chem. Soc.* **2010**, *132*, 4178−4190.

(26) Schröder, D.; Shaik, S.; Schwarz, H. *Acc. Chem. Res.* **2000**, *33*, 139−145.

(27) Zhao, Y.; Truhlar, D. G. *J. Chem. Phys.* **2006**, *125*, 194101−194118.

(28) Zhao, Y.; Truhlar, D. G. *Theor. Chem. Acc.* **2008**, *120*, 215−241.

(29) Fukui, K. *J. Phys. Chem.* **1970**, *74*, 4161−4163.

(30) Gonzalez, C.; Schlegel, H. B. *J. Chem. Phys.* **1989**, *90*, 2154−2161.

(31) Andrae, D.; Hüßermann, U.; Dolg, M.; Stoll, H.; Preuß, H. *Theor. Chim. Acta* **1990**, *77*, 123−141.

(32) Frisch, M. J.; Trucks, G. W.; Schlegel, H. B.; Scuseria, G. E.; Robb, M. A.; Cheeseman, J. R.; Scalmani, G.; Barone, V.; Mennucci, B.; Petersson, G. A.; Nakatsuji, H.; Caricato, M.; Li, X.; Hratchian, H. P.; Izmaylov, A. F.; Bloino, J.; Zheng, G.; Sonnenberg, J. L.; Hada, M.; Ehara, M.; Toyota, K.; Fukuda, R.; Hasegawa, J.; Ishida, M.; Nakajima, T.; Honda, Y.; Kitao, O.; Nakai, H.; Vreven, T.; Montgomery, J. A., Jr.; Peralta, J. E.; Ogliaro, F.; Bearpark, M.; Heyd, J. J.; Brothers, E.; Kudin, K. N.; Staroverov, V. N.; Kobayashi, R.; Normand, J.; Raghavachari, K.; Rendell, A.; Burant, J. C.; Iyengar, S. S.; Tomasi, J.; Cossi, M.; Rega, N.; Millam, J. M.; Klene, M.; Knox, J. E.; Cross, J. B.; Bakken, V.; Adamo, C.; Jaramillo, J.; Gomperts, R.; Stratmann, R. E.; Yazyev, O.; Austin, A. J.; Cammi, R.; Pomelli, C.; Ochterski, J. W.; Martin, R. L.; Morokuma, K.; Zakrzewski, V. G.; Voth, G. A.; Salvador, P.; Dannenberg, J. J.; Dapprich, S.; Daniels, A. D.; Farkas, Ö.; Foresman, J. B.; Ortiz, J. V.; Cioslowski, J.; Fox, D. J. *Gaussian 09*, revision D.01; Gaussian, Inc.: Wallingford CT, 2009.

(33) Ovchinnikov, A. A.; Labanowski, J. K. *Phys. Rev. A: At., Mol., Opt. Phys.* **1996**, *53*, 3946−3952.

(34) Weissbluth, M. *Atoms and Molecules*; Academic Press: New York, 1978; p 587.

(35) Scalmani, G. M.; Frisch, J. *J. Chem. Phys.* **2010**, *132*, 114110−114112.

(36) McQuarrie, D. A.; Simon, J. D. *Molecular Thermodynamics*; University Science Books: Sausalito, CA, 1999.

(37) Wertz, D. H. *J. Am. Chem. Soc.* **1980**, *102*, 5316−5322.

(38) Cheng, M.-J.; Nielsen, R. J.; Goddard, W. A., III *Chem. Commun.* **2014**, *50*, 10994−10996.

(39) Stephens, P. J.; Devlin, F. J.; Chabalowski, C. F.; Frisch, M. J. *J. Phys. Chem.* **1994**, *98*, 11623−11627.

DOI: 10.1021/acs.inorgchem.5b01832
Inorg. Chem. XXXX, XXX, XXX−XXX